JOURNAL OF GEOPHYSICAL RESEARCH, VOL. 95, NO. C10, PAGES 17,865–17,876, OCTOBER 15, 1990

Variations of Global Mesoscale Eddy Energy Observed From Geosat

C. K. SHUM, R. A. WERNER, D. T. SANDWELL,[1] B. H. ZHANG,[2] R. S. NEREM,[3] AND B. D. TAPLEY

Center for Space Research, The University of Texas at Austin

The global distribution of eddy kinetic energy has been synoptically observed from analysis of the Geosat Exact Repeat Mission (ERM) altimeter data collected for a 2-year period from November 1986 through November 1988. Using a technique developed by Sandwell and Zhang (1989), altimeter data from forty-four 17-day repeat cycles (2 years) were processed into sea surface slopes along the satellite ground track, averaged, and filtered to produce a mean sea surface slope profile having an estimated accuracy of 0.2 μrad (2 cm sea level change over 100 km distance). A series of global eddy kinetic energy maps, each averaged over 3 months, and their mean were then generated. The maximum mean eddy kinetic energy per unit mass exceeds 2000 cm^2/s^2 for most of the western boundary currents; however, it only reaches approximately 500 cm^2/s^2 for the Antarctic Circumpolar Current (ACC). More than 65% of the world ocean has relatively low variability with an eddy kinetic energy of less than 300 cm^2/s^2. Results obtained from this study are in general agreement with other Geosat ocean variability studies (e.g., Zlotnicki et al., 1989). However, significantly higher variability is found when compared with either Seasat or ship drift data. Significant seasonal variations were found in the Gulf Stream and Kuroshio currents. The ACC system exhibits no apparent seasonal variation.

INTRODUCTION

Ocean currents, in association with the influence of the atmosphere, move the Earth's heat from one latitude to another, delivering warm water to the colder climates and cold water from the polar regions to the warm equatorial regions. Over the last 2 decades, substantial research efforts have been focused on the variability of the ocean currents. *Wyrtki et al.* [1976] showed that fluctuating currents contain far more kinetic energy than does the mean motion. Recent variability studies have classified wavelike and turbulent motions, assessed their role in ocean dynamics, estimated the importance of the various instabilities of the mean motion of the currents, and calculated the interactions among wave fields of the major currents [*Stewart*, 1985; *Robinson*, 1983; *Douglas et al.*, 1983].

In the past, oceanography has depended on sparse measurements collected from surveying ships, buoys, and tide gauges to study the ocean eddy field variability. Experience with GEOS-3 [*Stanley*, 1979] and Seasat [*Tapley and Born*, 1980; *Tapley et al.*, 1982] during the 1970s demonstrated the potential of satellite altimetry, but neither mission provided a data set that was both sufficiently long term and globally distributed to allow the synoptic mapping of oceanographic features. The United States Navy's Geosat Exact Repeat Mission (ERM) [*McConathy and Kilgus*, 1987], initiated on November 8, 1986, was primarily dedicated to the study of mesoscale oceanographic features. The Geosat ERM ground track repeats every 17 days, and the equatorial ground track spacing is about 160 km, providing global coverage. Its high quality (5-cm precision) height measurements and its good spatial and temporal coverage provide a unique opportunity to study detailed and long-term oceanographic phenomena. Previous studies used altimeter data from GEOS-3, Seasat, and Geosat for the synoptic mapping of the mesoscale (50- to 1000-km wavelength) oceanographic features and have demonstrated its potential [*Cheney et al.*, 1983; *Douglas et al.*, 1983; *Menard*, 1983; *Fu*, 1983*a*, *b*; *Fu et al.*, 1987; *Fu and Zlotnicki*, 1989; *Zlotnicki et al.*, 1989; *Sandwell and Zhang*, 1989].

This investigation uses a new technique [*Zhang*, 1988; *Sandwell and Zhang*, 1989] to extract global mesoscale (50- to 1000-km wavelength) oceanic variability from collinear Geosat altimeter profiles which have large radial orbit error (~4 m). A simple derivative filtering process suppresses long wavelength (>10,000 km) orbit error, as well as other long wavelength errors [*Zhang, 1988*]. Two years of Geosat data were processed and averaged into a mean slope profile. Temporal evolutions of mesoscale variability about the mean were computed using the altimeter-derived along-track slopes. Global eddy kinetic energy per unit mass for the mesoscale variability can then be estimated from the slope variability, but several assumptions related to isotropy and sampling are required to implement this approach. The resulting product is a series of global mesoscale eddy kinetic energy maps with a time scale which can vary from days to months. The 2-year mean eddy kinetic energy map was also generated for the period from November 1986 through November 1988.

Maps of eddy kinetic energy were generated for the major current systems averaged over 3-month intervals to examine the seasonal variations of some of the current systems. The more rapid temporal evolution of eddies was examined at 10-day intervals for the Agulhas retroreflection region south of Africa using the Geosat time series. The seasonal variations of eddy energy for the Gulf Stream, the Kuroshio, and the Antarctic Circumpolar Current (ACC) were synoptically observed and compared with recent studies. The rapid energetic variations of eddy motions in the Agulhas region was also compared with recent studies. This paper will demonstrate the ability of satellite altimetry to provide temporal (days) and spatial (150 km) resolution for the mapping of sea surface variability.

ALTIMETER DATA PROCESSING AND ANALYSIS

Data Processing

The first 44 of the 17-day repeat cycles of the Geosat altimeter geophysical data record (GDR), which spans November 8, 1986,

[1]Now at Scripps Institute of Oceanography, La Jolla, California.
[2]Now at Space Science and Applications Research Center, Chinese Academy of Sciences, Beijing, People's Republic of China.
[3]Now at Goddard Space Flight Center, Greenbelt, Maryland.

Paper number 90JC00961.
0148-0227/90/90JC-00961$05.00

through November 24, 1988, were used in the analysis. The global data coverage in this data set is shown in Figure 1.

The Geosat altimeter data were first edited according to criteria [*Zhang*, 1988] based on previous experience with the Seasat altimeter data: automatic gain control greater than 34 DB or less than 15 DB, all data on land or on ice, standard deviation of once-per-second height average exceeding 0.1 m, and significant wave height greater than 8 m. This edit criteria eliminated about 4% of the total data.

Then the 10-per-second altimeter height observations were averaged into two-per-second observations. The two-per-second sampling rate retains more of the short wavelength information needed for interpolation than the one-per-second data. Corrections for ocean and solid Earth tides and for ionospheric and tropospheric propagation (wet and dry component from the Fleet Numerical Oceanographic Center (FNOC)) were then applied to the two-per-second data. The inverted barometric correction (1 cm/mbar) was applied to the data using the FNOC pressure data. The data were then divided into ascending and descending passes. These passes were further divided whenever a data gap exceeding 10 s was detected. Along-track derivatives (slopes) of each altimeter height profile were computed for the 44 repeat cycles (approximately 60 million observations). The slope profiles were averaged into a mean profile, and individual slope profiles were compared against the mean profile to perform additional editing. At each point, individual slopes which were further than 4 standard deviations from the mean slope were edited, and the mean was recomputed. This procedure removed about 0.8% of the total data.

Temporal evolution of slope variability can be computed by differencing each slope profile from the mean slope. The time series of eddy kinetic energy can be computed from the slope variability. Energy maps of mesoscale variability can be generated for temporal scales from several days to months within the 2-year Geosat data span.

Filtering

The final step in the processing was to low-pass filter the data. This procedure is necessary (1) to eliminate the very short wavelength altimeter noise and high frequency geoid signals [*Sandwell and Zhang*, 1989] and (2) to effectively interpolate into areas where no data were available and to output evenly gridded data. A Gaussian filter of the form $\exp(-\Delta t^2 / 2\sigma^2)$ was used following *Sandwell and Zhang* [1989], where Δt is the time difference from the center of the filter to each point, and $\sigma = 5$ s, which corresponds to a 150-km half-amplitude cutoff. The filter window extended 3σ in both directions. Bins with no data were interpolated from surrounding bins, provided the corresponding weights exceed a 90% threshold.

Power spectrum analysis using Seasat and Geosat data have indicated that the oceanic variability has little power at wavelengths shorter than 50 km owing to altimeter noise [*Fu*, 1983*a*; *Fu and Zlotnicki*, 1989]. The filtering reduces the root-mean-square (rms) standard deviation of the mean profile from 1 μrad to 0.2 μrad, corresponding to 2 cm in sea level change over 100-km distance. The analysis of filtering Geosat data is described in detail by *Zhang* [1988].

Error Sources

Sandwell and Zhang [1989] demonstrated that the derivative technique has several advantages over the conventional "bias and tilt" technique for the analysis of collinear altimeter data: (1) the derivative method effectively removes long-wavelength orbit

Fig. 1. GEOSAT ERM Altimeter Data (November 1986 - November 1988)

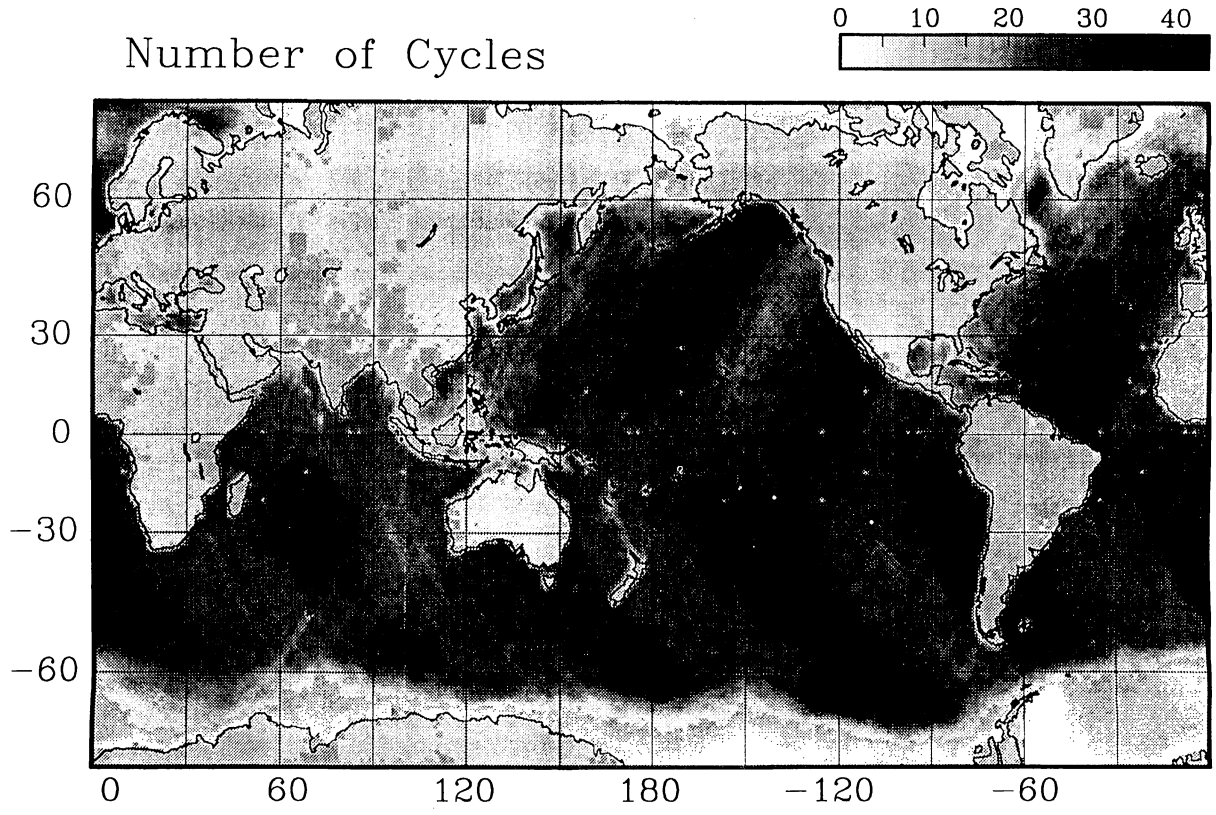

Fig. 1. Geosat ERM global altimeter data coverage from November 1986 through November 1988.

error and has no edge effects, and (2) the derivative method conveniently produces the dynamic slope of the sea surface, which is proportional to the current velocity, assuming geostrophic balance. The long wavelength orbit error is shown to be diminished using the derivative technique by *Sandwell and Zhang* [1989]. Spectral analysis using differenced profiles has shown that the expected power of once-per-revolution orbit error is less than 0.1 μrad (1 cm over 100 km), and that the relative error at other wavelengths is less than 0.05 μrad. These analyses have shown that the relative error among Geosat repeat slope profiles is accurate to about 0.1–0.2 μrad (1–2 cm over 100 km) for the study of mesoscale variability. The 2-year mean profile is probably accurate to better than 0.2 μrad.

The repeat track method assumes the repeat cycles are collinear (repeat ground tracks within ±1 km). Large cross-track geoid gradients associated with oceanic trenches and seamounts will introduce false signals [*Brenner et al.*, 1990]. Care must be taken to interpret oceanographic phenomena near these areas. However, the geoid gradients rarely exceed 100 μrad, which would cause a false signal of about 3 cm over 100 km [*Sandwell and Zhang*, 1989], making noncollinearity less of a problem.

Fu and Zlotnicki [1989] show that the effects of errors induced by water vapor are relatively small compared with the mesoscale signals shorter than 100-km wavelength. However, strong individual water vapor anomalies can occasionally affect the detection of ocean eddies. The Geosat altimeter data used in this study were collected during a minimum in the 11-year cycle of the ionospheric activities, resulting in diminished errors in the ionospheric range delay correction to the altimeter data.

The use of the inverted barometer correction could result in errors of a few centimeters, especially in the upper and lower latitudes, where the meteorological models and sea level pressure are less accurate. In addition, large ocean tide errors can produce variations in sea surface slope, especially in the coastal areas like the Amazon shelf and the Yellow Sea [*Sandwell and Zhang*, 1989]. In this study, care was taken to edit high slope variability due to possible tide error near the coastal areas; however, further study is warranted to assess the contribution of tide model error.

COMPUTATION OF EDDY KINETIC ENERGY

Geostrophic equilibrium is a first-order solution of the fundamental Navier-Stokes hydrodynamic equations for a rotating homogeneous fluid. It states that the horizontal velocity field is obtained from a balance between the Coriolis force and the pressure gradient. The connection between currents and surface topography can be obtained by solving the hydrodynamic equations assuming geostrophic balance and hydrostatic equilibrium [e.g., *Wunsch and Gaposchkin*, 1980]. The relative velocity can be obtained by integrating vertically from an arbitrary reference level z_r to obtain

$$v - v_r = \frac{g}{\rho f} \int_{z_r}^{0} \frac{\partial \rho}{\partial z}\, dz \tag{1}$$

where v_r is the velocity at the reference level and v is the velocity at the ocean surface, ρ is the water density, g is the gravitational acceleration, and the Coriolis parameter $f = 2\Omega \sin\phi$ is related to the rotation rate of the Earth, where Ω is the rotation rate and ϕ is the latitude.

Satellite altimetry has a potential for determining absolute geostrophic velocity. Instead of assuming the velocity at depth or taking measurements deep into the ocean, the reference level can be chosen as a long-term averaged sea surface relative to a geoid which can be measured by satellite altimetry. No assumption is necessary about the surface velocity because it is related to the surface elevation through the geostrophic and hydrostatic equations by

$$v = \frac{g}{f} \frac{\partial \eta}{\partial x} \tag{2}$$

where v is the surface velocity and η is the elevation of the ocean surface with respect to the geoid measured directly by satellite altimetry; x is in a horizontal direction perpendicular to v. If the altimeter measurements are corrected for the effects of the tides and atmospheric load, the remaining ocean surface topography η is primarily composed of two components: (1) a large-scale component associated with the quasi-stationary mean circulation, which can be considered time-invariant for the period under consideration, and (2) a mesoscale component associated with the eddy circulation, which is time-varying and appears at the surface as sea height changes or eddy dynamic heights [*Menard*, 1983]. To be consistent with the eddy height, the sea surface slope changes are hereinafter referred to as the eddy slope.

If altimeter passes are collinear, as is the case for Geosat ERM, the along-track slope $\Delta\, \partial\eta^i / \partial x$ can be expressed for each repeated measurement i as follows:

$$\Delta \frac{\partial \eta^i}{\partial x} = \frac{\partial \eta^i}{\partial x} - \left[\frac{\partial \eta}{\partial x}\right]_m \tag{3}$$

where x is the distance along the altimeter profile, $\partial\eta^i / \partial x$ is the sea surface slope of repeat cycle i, and $(\partial\eta / \partial x)_m$ is the slope of the average of the repeated profiles for the 2-year time period. By using the along-track profile, the time-independent effects of the gravity field and long-wavelength mean circulation are eliminated.

Let the quantity Δv be the deviation from the mean associated with the eddy flow, which by analogy is called eddy velocity. The component of eddy velocity Δv in the satellite cross-track direction y can be determined from the eddy slope $\Delta\, \partial\eta^i / \partial x$ in the along-track direction x for profile i. The geostrophic relation gives

$$\Delta v_y^i = \frac{g}{f} \Delta \frac{\partial \eta^i}{\partial x} \tag{4}$$

where Δv_y^i is the eddy velocity in the cross-track direction.

The rms velocity variability $\bar{\sigma}^2(v_y)$ in the cross-track direction y can be defined by

$$\bar{\sigma}^2(v_y) = \frac{\sum_{i=1}^{n} \left[\Delta v_y^i\right]^2}{n} \tag{5}$$

where n is the number of repeat slope measurements. The eddy kinetic energy E_e is approximately the average of eddy velocity rms in both the along-track and cross-track directions

$$E_e = \tfrac{1}{2}\left[\bar{\sigma}^2(v_x) + \bar{\sigma}^2(v_y)\right] \tag{6}$$

One of the ways to compute the eddy kinetic energy with altimetry is to assume that the velocity variability is isotropic

$$\bar{\sigma}^2(v_x) = \bar{\sigma}^2(v_y) = \bar{\sigma}_v^2 \tag{7}$$

where the $\bar{\sigma}_v^2$ is the total rms velocity variability. Then the eddy kinetic energy is simply

$$E_e = \bar{\sigma}_v^2 \tag{8}$$

In this study, we assumed that the eddy field is isotropic. Exceptions to isotropy occur in the Gulf Stream and in the southern ocean where the principal axes of variance sometimes parallels its direction of flow. By averaging over a certain period, e.g., 10 days, it is possible to obtain enough altimeter data over a

gridded area for both ascending and descending passes, from which the determination of current velocity direction may be possible. This is particularly favorable where the closer spacing of ground tracks in the regions of higher and lower latitudes provides more data and higher resolution.

EDDY KINETIC ENERGY MAPS FOR GLOBAL MESOSCALE VARIABILITY

The 2-year global eddy kinetic energy maps are shown in Plate 1. (Plates 1–5 are shown here in black and white. The color versions can be found in the separate color section in this issue.) The global eddy kinetic energy map was computed by averaging both ascending and descending passes. Data were gridded into ½°×½° bins and smoothed using a Gaussian filter of the form $\exp(-r^2/2\sigma^2)$, where r is the distance from the center of the filter to each outlying point and σ was chosen to be 1°. The filter window was 5.5°. This same filter was used to interpolate bins containing no data. To ensure that isolated data points did not significantly influence surrounding areas which have no data, the sum of weights corresponding to data points have to exceed a 20% threshold before a "no-data" point was replaced. The along-track resolution is approximately 32.5 km (12-per-minute data rate). The ground track spacing, which is approximately 160 km at the equator, decreases with higher and lower latitudes. For example, the spacing decreases to approximately 110 km at ±45°, 80 km at ±60°, and 55 km at ±70°. An output resolution of ½°×½° was chosen after (1) experimentation with 2° resolution, which yields virtually identical results; (2) choosing appropriate filtering constants to insure that no false signals were generated because of data outages; and (3) noting that more detail is observed, especially for the high-variability regions.

The color scale indicates the intensity of the mesoscale eddy kinetic energy per unit mass, ranging from light blue (20 cm^2/s^2) to yellow (2000 cm^2/s^2). The color scale is made to be logarithmic to enhance low and high values of the energy. Eddy kinetic energy above 2000 cm^2/s^2 is white. The purpose is to avoid the singularity encountered in the geostrophic assumption near the equator. At ±5° latitude, the maximum magnitude of the eddy kinetic energy reaches approximately 5000 cm^2/s^2. From ±5° to the equator, the maximum magnitude increases by an order of magnitude per degree as the equator is approached. Although *Wyrtki et al.* [1976] have also shown very high values of eddy energy (>1000 cm^2/s^2) near the equatorial region, the Geosat eddy kinetic energy computed here is orders of magnitude larger. It is unlikely that these high energy values are real. They are likely due to the singularity of the geostrophic assumption at the equator.

Plate 1*a* (as well as subsequent figures) combines data from the ascending and descending passes, while Plates 1*b* and 1*c* were generated from only the ascending or descending passes, respectively. The close similarity of these figures supports the isotropic assumption, i.e., that the magnitude of the variability at each point is approximately equal in all horizontal directions.

Plate 1 shows that the highest variations in eddy energy occur over the western boundary currents, such as Agulhas, Gulf Stream, Kuroshio, East Australian, and Brazilian currents. The maximum magnitude of these high variations is greater than 2000 cm^2/s^2, corresponding to approximately 30- to 40-cm sea level changes. The ACC produces relatively low mesoscale variations of approximately 300 cm^2/s^2 to 500 cm^2/s^2. Variabilities are generally low in the southeastern Pacific and Atlantic, corresponding to variations of about 100–200 cm^2/s^2. More than 65% of the world ocean is found to have relatively low eddy kinetic energy (<300 cm^2/s^2). This result is consistent with *Cheney et al.* [1983] and *Sandwell and Zhang* [1989]. The loop current is evident in the Gulf of Mexico where the eddy kinetic energy reaches approximately 2000 cm^2/s^2. High eddy kinetic energies which occur on shallow shelves, such as the Amazon Shelf, the Yellow Sea, the Timor Sea (northeast Australia), the Great Barrier Reef, and the Bristol Bay (southeast Alaska), are suspected to be due to ocean tide error. This phenomenon was also observed by *Zhang* [1988], *Sandwell and Zhang* [1989], and *Zlotnicki et al.* [1989].

The 2-year Geosat eddy kinetic energy map compares well qualitatively with the map generated by *Wyrtki et al.* [1976] using ship drift data. However, the Geosat map shows significantly higher maximum values of eddy kinetic energy when compared with the *Wyrtki et al.* [1976] result. For example, maximum values of approximately 2000 cm^2/s^2 were found for the Kuroshio, Agulhas, and East Australian currents from the Geosat map. The ship drift energy map shows values of only about 1000 cm^2/s^2 for these regions. It is noted that the Wyrtki map is averaged over a larger area and includes ageostrophic flow.

In general, the Geosat-derived eddy kinetic energy map is qualitatively similar to the height variability maps derived using 1 month of Seasat data [e.g., *Cheney et al.*, 1983]. However, Geosat results show improved temporal coverage (2 years) and spatial resolution (Figure 1*a*) because Geosat has a ground track sampling of approximately 160 km (17-day repeat orbit) at the equator instead of the 930-km sampling (3-day repeat orbit) for Seasat. Higher variability was found in the Geosat results than in the Seasat results reported by *Cheney et al.* [1983] and by *Menard* [1983] for some of the major current systems. For example, the Geosat results show higher values of eddy kinetic energy (1000–2000 cm^2/s^2) over a broader region (east longitude from 285° to 310°) for the Gulf Stream than is reported by *Menard* [1983]. The Geosat eddy kinetic energy values for the Kuroshio Current are found to be significantly higher than the Seasat results obtained by *Menard* [1983] (2000 cm^2/s^2 versus 1000 cm^2/s^2 maximum magnitude). The improved spatial and temporal data sampling for Geosat may have allowed better resolution of broader spectrum of mesoscale signals.

With the exception of the equatorial region, the 2-year Geosat eddy kinetic energy map is also in good agreement with the sea surface height map generated by *Zlotnicki et al.* [1989], which used 1.3 years of Geosat data. For example, the average sea level variability for the Agulhas Current from *Zlotnicki et al.* [1989] is approximately 24 cm, corresponding approximately to the average eddy kinetic energy of 1500 cm^2/s^2 obtained in this study. For the Gulf Stream, an average sea level variability of 20 cm obtained by *Zlotnicki et al.* [1989] is also in good agreement with the average energy value of 1100 cm^2/s^2 found in this investigation. The magnitude and shape of the 2-year mean eddy kinetic energy for the Gulf Stream also compare remarkably well with the eddy kinetic energy map generated by *Le Traon and Rouquet* [1990] for the same region using Geosat data.

SEASONAL VARIATION OF EDDY FIELDS

Maps of eddy kinetic energy averaged over approximately 3-month intervals were generated for the Gulf Stream region (shown in Plates 2*a–h*), the Kuroshio Extension region (Plates 3*a–3h*), and the Antarctic region (Plates 4*a–4h*). The maps showing the Antarctic region used a polar projection to show the ACC, Agulhas Current, Falkland, and Brazilian currents and the East Australian Current. In general, the maps show good spatial resolution with the exception of data outages in the Gulf Stream

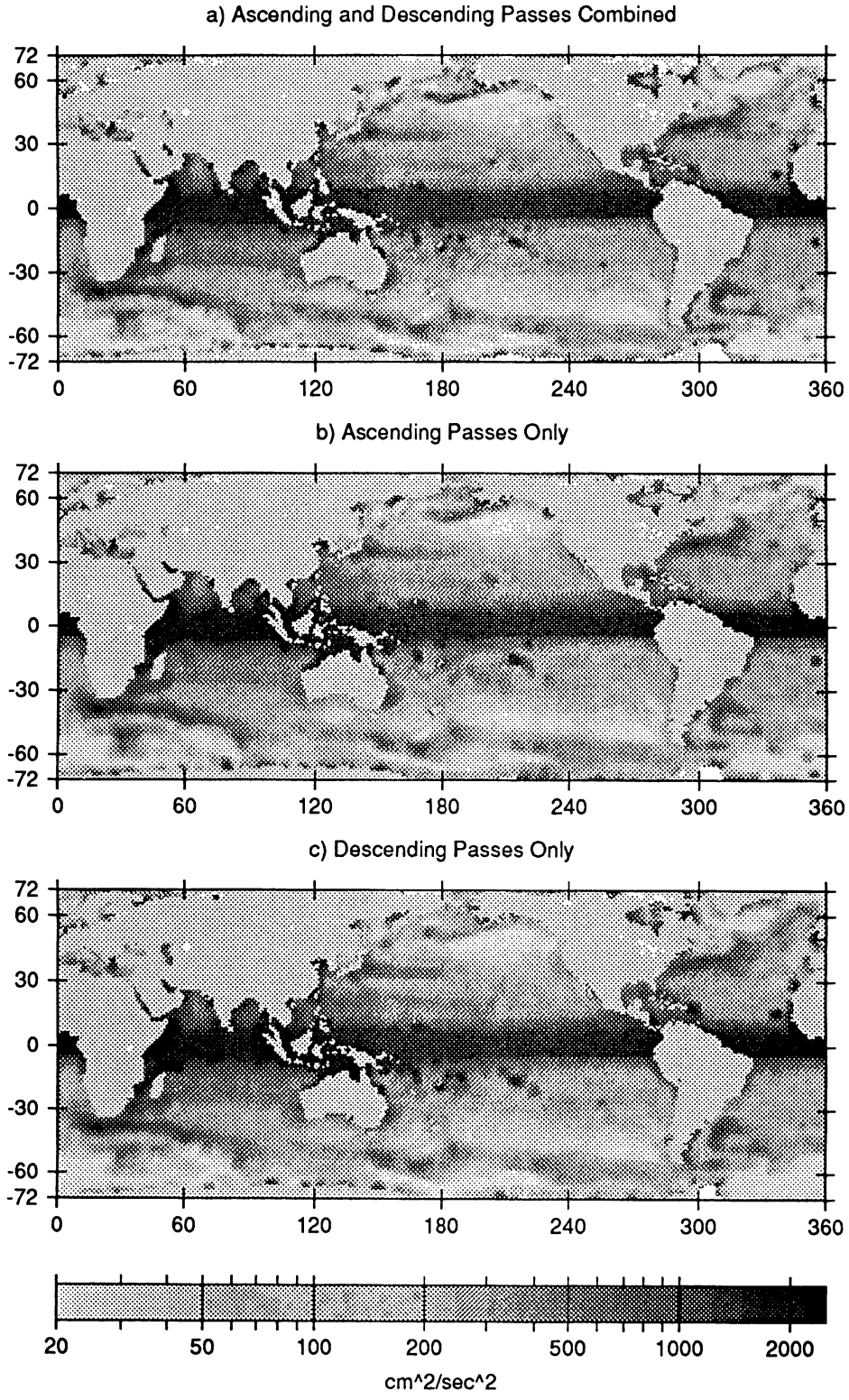

Plate 1. Eddy kinetic energy maps generated using 2 years of Geosat altimeter data (November 1986 through November 1988) for (*a*) ascending and descending passes, (*b*) ascending passes only, and (*c*) descending passes only. Similarities between Plates 1*b* and 1*c* support the isotropic assumption that along-track and cross-track rms velocity variability are identical. (The color version of this figure can be found in the separate color section in this issue.)

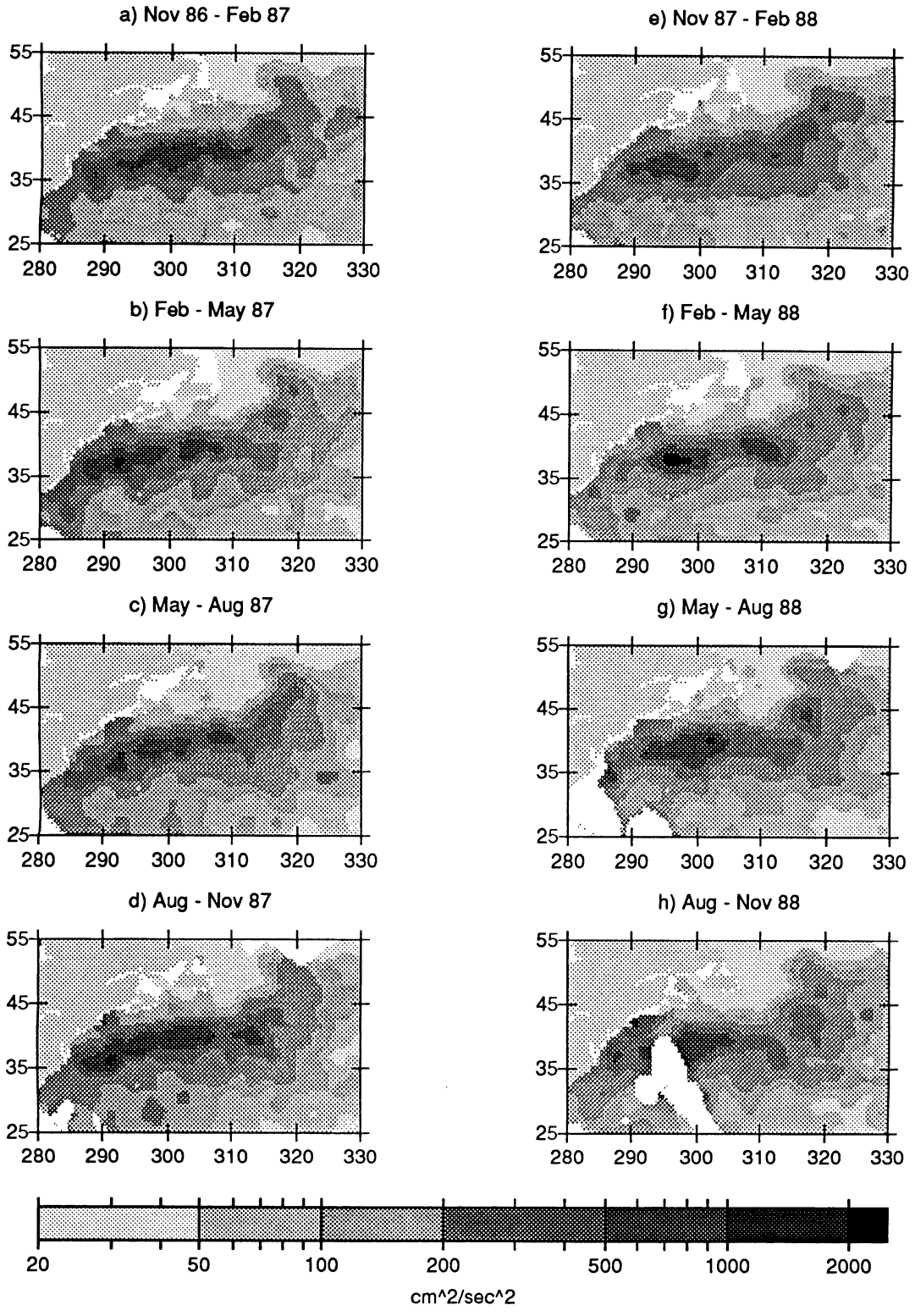

Plate 2. (*a–h*) Eddy kinetic energy maps averaged over 3-month intervals for the Gulf Stream current system. The Gulf Stream seems delineated by 500-cm^2/s^2 eddy kinetic energy levels. Annual cycles of average position and shape are evident, but strength and location of maximum variability do not repeat. (The color version of this figure can be found in the separate color section in this issue.)

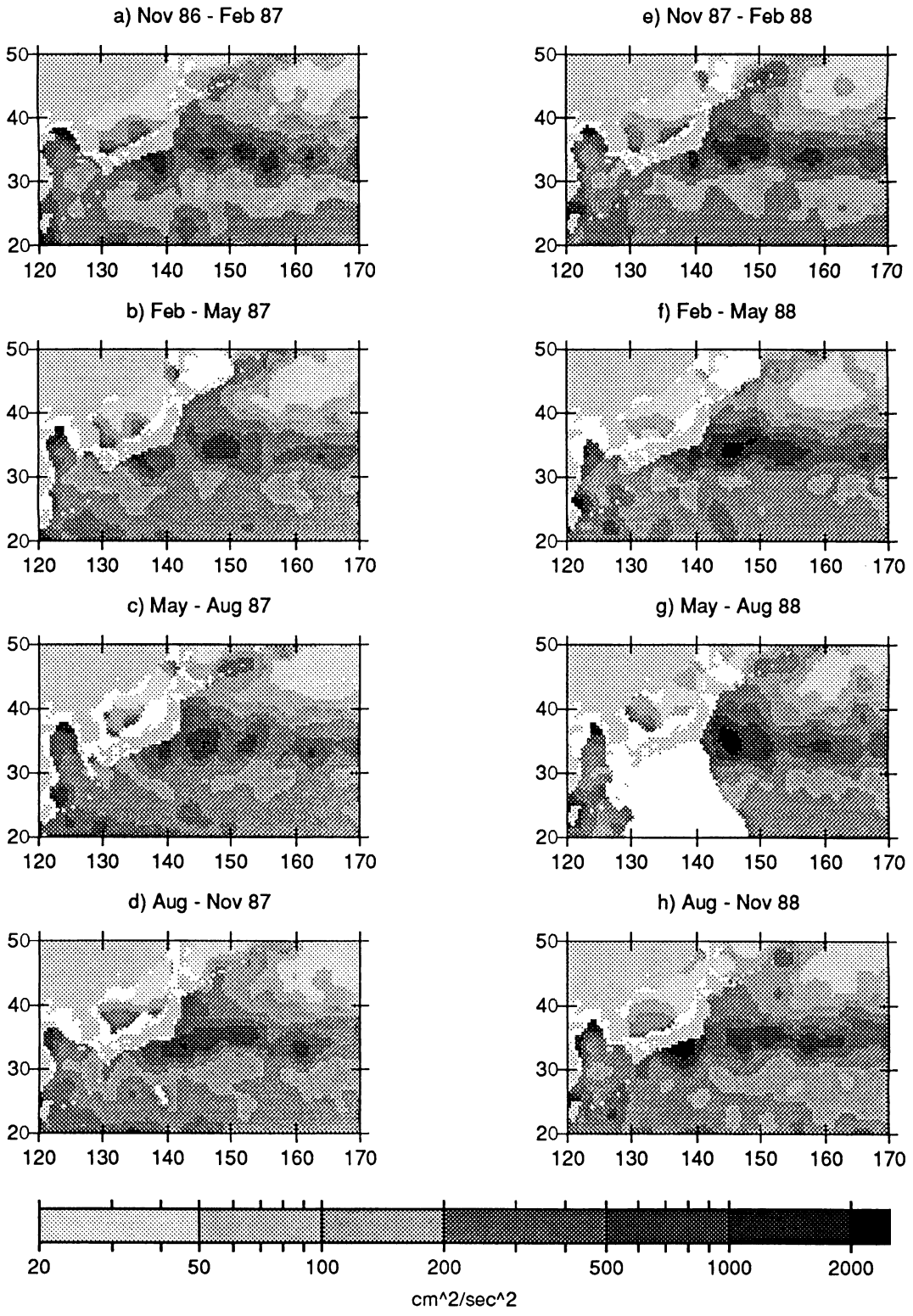

Plate 3. (*a–h*) Eddy kinetic energy maps averaged over 3-month intervals for the Kuroshio current. High values of eddy kinetic energy (>1000 cm^2/s^2 correspond to the meandering of the current front, especially between the Kuroshio and Oyashio fronts (35°–40° N, 140°–155° E). (The color version of this figure can be found in the separate color section in this issue.)

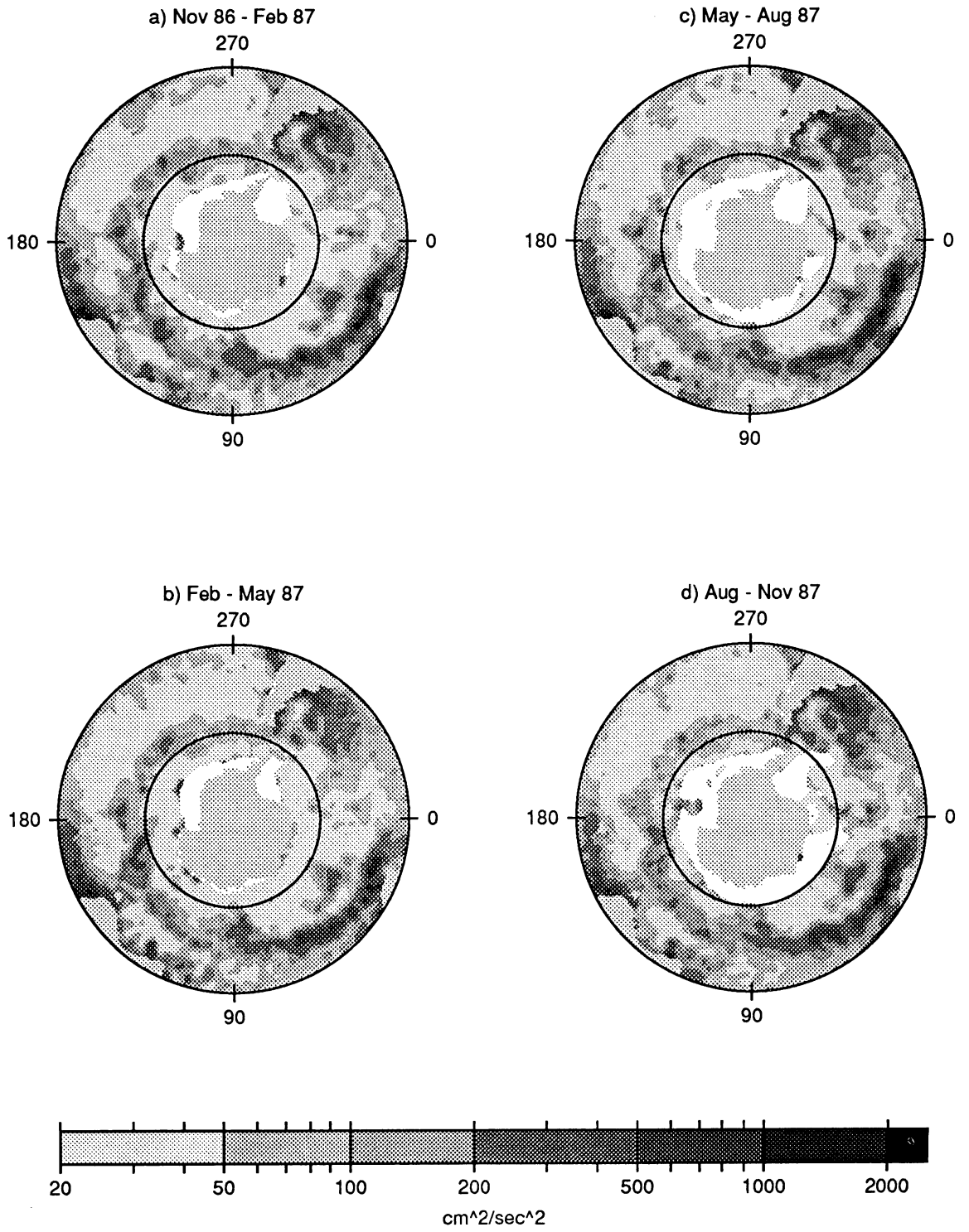

Plate 4. (*a–h*) Eddy kinetic energy maps averaged over 3-month intervals for the Antarctic region. Eddy kinetic energy in the Antarctic Circumpolar Current generally reaches 500 cm^2/s^2, and energies exceeding 1000 cm^2/s^2 appear in the Agulhas, Brazilian, and East Australian currents. There seems to be little seasonal variation in the position and magnitude of the ACC's eddy kinetic energy. (The color version of this figure can be found in the separate color section in this issue.)

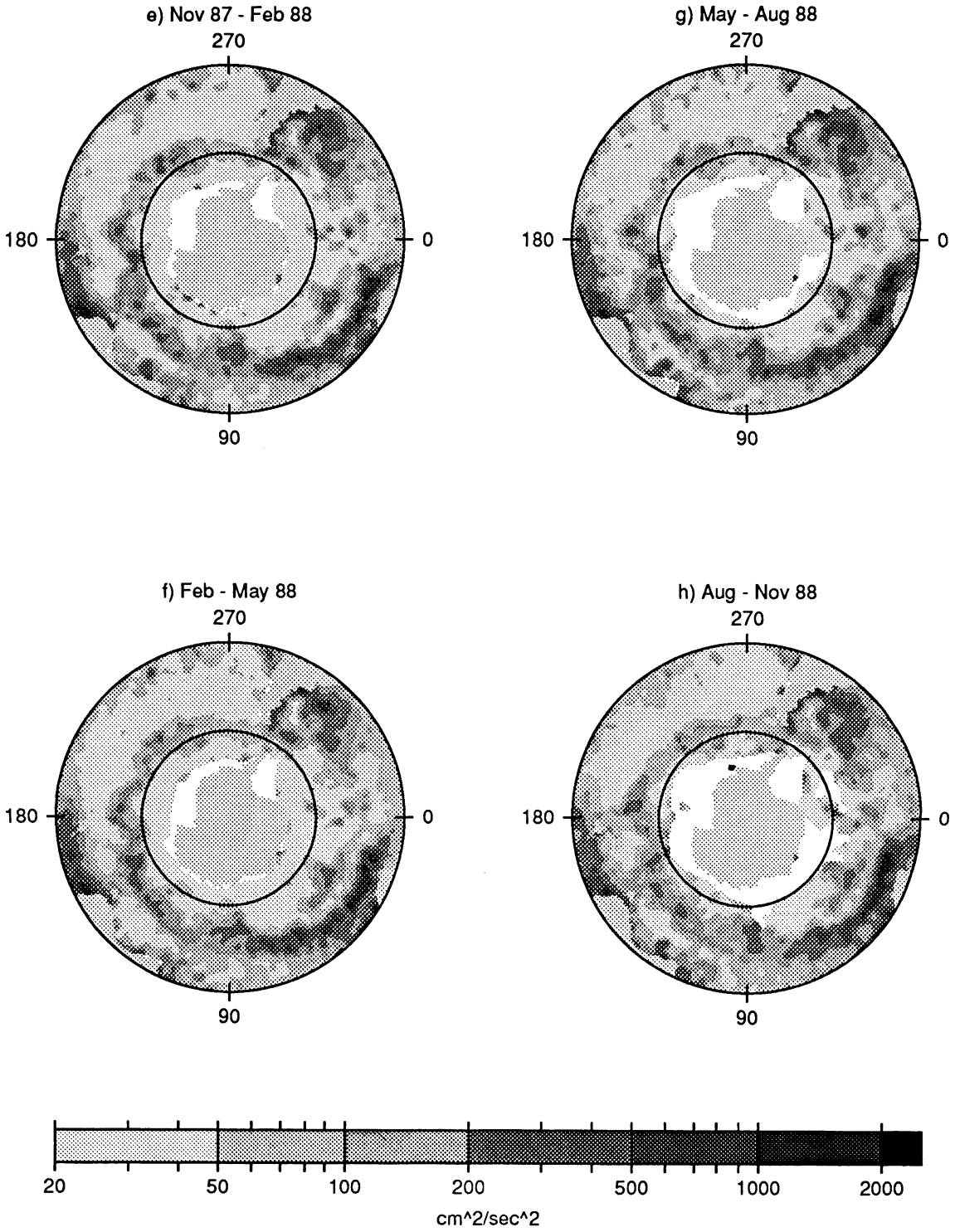

Plate 4. (continued)

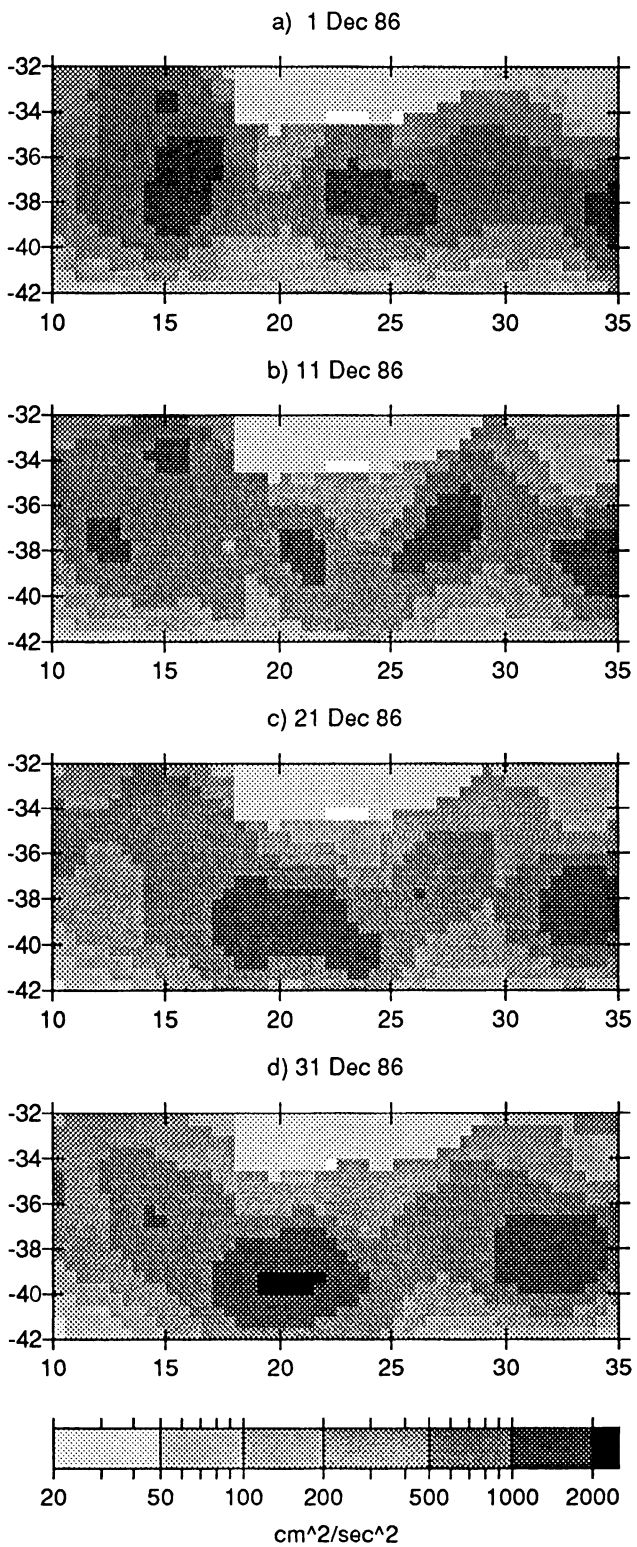

Plate 5. (*a–d*) Eddy kinetic energy snapshots generated at 10-day intervals for the Agulhas retroreflection region. Eddy features evolve quickly in strength and position. (The color version of this figure can be found in the separate color section in this issue.)

during August–November 1988 (Plate 2*h*) and in the Kuroshio current during May–August 1988. These two data outages affect areas approximately of size 10° × 10°.

Gulf Stream

Plates 2*a*–2*h* show the 3-month averaged eddy kinetic energy maps of the Gulf Stream for the 2-year Geosat data span. In general, the Gulf Stream is delineated by eddy kinetic energy values greater than 500 cm^2/s^2, with isolated peaks of 1500–2000 cm^2/s^2 occurring between 290° and 320° in east longitude. Eddy kinetic energy drops to below 500 cm^2/s^2 north of the Gulf Stream at the shelf break, which also coincides with the northern limit of the warm ring region. The 500 cm^2/s^2 contour terminates at 30°N; cold rings are not normally found below this latitude.

Plates 2*a*–2*h* display high variations of the Gulf Stream from season to season in both the position of the mean current system and the magnitude of peaks of high variability. The maximum differences of eddy kinetic energy for each of the 3-month averages subtracted from the 2-year mean are approximately ±300 cm^2/s^2. The position of the Gulf Stream varies noticeably with the season; the path tends to shift northward several degrees in latitude in the summer/fall season and southward by approximately the same distance in the winter/spring season. This result seems to be consistent with the results obtained by *Fu et al.* [1987] using 3.5 years of GEOS-3 altimeter data.

The position of the Gulf Stream shows remarkable similarity for each season of 1987 and 1988, indicating clear annual variation patterns. The average current positions and shapes for each of the four seasons for 1987 are similar to each of the seasons for 1988. However, the peak magnitudes and their locations seem to vary between each season for the two different years. Between 310° and 320° E, the 1000-cm^2/s^2 energy contour of the Gulf Stream is found to extend upward to around 45° latitude during the winter and summer seasons (Plates 2*a* and 2*e* and Plates 2*c* and 2*g*, respectively). The contour drops to around 40° latitude during the spring and autumn seasons (Plates 2*b* and 2*f* and Plates 2*d* and 2*h*, respectively). These features show clear semiannual variations.

Kuroshio Current

Plates 3*a*–3*h* show the 3-month averaged kinetic energy maps of the Kuroshio Current for the 2-year Geosat data span. In general, high kinetic energy values (>1000 cm^2/s^2) associated with the Kuroshio Current were found, corresponding to the meandering of the current front. This signature is especially evident between the Kuroshio front and the Oyashio front (35°–40° in latitude, 140°–155° in longitude), a confluence zone where eddy activity is high. The general shape of the Kuroshio Current is in general agreement with the Seasat-derived maps generated by *Menard* [1983]; however, the magnitude of the Geosat results is significantly higher than that of Menard's results.

Differences of the 3-month averaged eddy kinetic energy from the 2-year mean were computed to assess the seasonal variations of the Kuroshio Current. Again, there is notably high seasonal variability in the magnitude due to the meandering of the Kuroshio Current. However, the shape and the position of the Kuroshio Current show similarity for each season of 1987 and 1988, indicating annual patterns. The largest seasonal differences from the 2-year mean are about ±300 cm^2/s^2.

Southern Ocean

Plates 4*a*–4*h* show the 3-month averaged kinetic energy maps of the Antarctic region for the 2-year Geosat data span. In general, the kinetic energy values for the ACC generally reach the 500-cm^2/s^2 level, although higher variability is found in the Agulhas, Brazilian, and East Australian currents. The energetic eddy motions are highly variable in the Agulhas Current region owing to the unsteady retroreflection of the current system [*Lutjeharms and Gordon*, 1987]. In addition to the Agulhas retroreflection region, the Brazilian Current and the East Australian Current also have high variability with kinetic energy values exceeding 1000 cm^2/s^2.

High seasonal variability is most evident in the Agulhas, Brazilian, and East Australian currents. There seems to be little variation from season to season for the Antarctic Circumpolar Current both in position and magnitude of the eddy energy during the 2-year Geosat data span. This result is consistent with the study reported by *Chelton et al.* [this issue] using Geosat data analysis for the southern ocean.

Agulhas Return Current

To examine the meandering and eddy-shedding of the Agulhas Current, four 10-day snapshots of eddy kinetic energy maps were generated for the dates December 1, December 11, December 21, and December 31, 1986. These maps are shown in the vicinity of the Agulhas retroreflection region (Plates 5*a*–5*d*). Several highly variable eddies features can be observed. The eddies to the east of 25° east longitude are mostly caused by the meandering and eddy shedding of the Agulhas Return Current, and the eddies to the west of 17° are probably warm eddies [*Fu and Zlotnicki*, 1989]. The eddy (20° east longitude) was observed to be intensifying with its eddy kinetic energy exceeding the magnitude of 2000 cm^2/s^2 on December 31, 1988. This result compares well with *Fu and Zlotnicki* [1989].

CONCLUSIONS

This paper presents the first global distribution of eddy kinetic energy and its temporal variations using multiyear satellite altimeter data from Geosat. Variations in sea surface slope for 2 years of Geosat altimeter data were computed by differencing the individual repeat slope profiles from the mean profile, and maps of eddy kinetic energy were computed. The mean mesoscale variability is estimated to have an accuracy of about 0.2 μrad, corresponding to a 2-cm sea level change over 100 km distance. More than 65% of the world ocean displays relatively low variability with eddy kinetic energy value less than 300 cm^2/s^2. Seasonal maps of eddy kinetic energy were averaged over 3-month intervals. For the major ocean current systems, significantly higher values of mesoscale variability were found in this study than the values reported by analyses of Seasat and ship drift data. There is good agreement when compared with other Geosat-derived mesoscale variability studies. Seasonal variations were examined and detected for the Gulf Stream and the Kuroshio Currents. The Antarctic Circumpolar Current does not seem to exhibit variations from season to season for the 2-year Geosat data span. By using a finer temporal scale at 10-day intervals, it is demonstrated that highly energetic eddy motions in the Agulhas retroreflection region are observable using Geosat data.

Acknowledgments. This research was supported partially by NASA Jet Propulsion Laboratory contract JPL 958122 and by the State of Texas Advanced Technology program. Additional computing resources for this work were provided by the University of Texas System Center for High Performance Computing. Valuable discussions with John Ries and Victor Zlotnicki are acknowledged. We particularly appreciate the helpful comments of Chet Koblinsky.

REFERENCES

Brenner, A. C., C. J. Koblinsky, and B. D. Beckley, A preliminary estimate of geoid-induced variations in repeat orbit satellite altimeter observations, *J. Geophys. Res.*, *95*(C3), 3033–3040, 1990.

Cheney, R. E., J. G. Marsh, and B. D. Beckley, Global mesoscale variability from collinear tracks of Seasat altimeter data, *J. Geophys. Res.*, *88*(C7), 4343–4354, 1983.

Chelton, D. B., M. G. Schlax, D. L. Witter, and J. G. Richman, Geosat altimeter observations of the surface circulation of the southern ocean, *J. Geophys. Res.*, this issue.

Douglas, B. C., R. E. Cheney, and R. W. Agreen, Eddy energy of the northwest Atlantic and Gulf of Mexico determined from GEOS-3 altimetry, *J. Geophys. Res.*, *88*(C14), 9595–9603, 1983.

Fu, L. L., On the wave number spectrum of oceanic mesoscale variability observed by the Seasat altimeter, *J. Geophys. Res.*, *88*(C7), 4331–4341, 1983*a*.

Fu, L. L., Recent progress in the applications of satellite altimetry to observing the mesoscale variability and general circulation of the oceans, *Rev. Geophys.*, *21*(8), 1657–1666, 1983*b*.

Fu, L. L., and V. Zlotnicki, Observing oceanic mesoscale eddies from Geosat altimetry: Preliminary results, *Geophys. Res. Lett.*, *16*(5), 457–460, 1989.

Fu, L. L., J. Vazquez, and M. E. Parke, Seasonal variability of the Gulf Stream from satellite altimetry, *J. Geophys. Res.*, *92*(C1), 749–754, 1987.

Le Traon, P., M. Rouquet, and C. Boissier, Space time scales of mesoscale variability in the North Atlantic as deduced from Geosat data (abstract), *Eos Trans. AGU*, *71*(2), p. 159, 1990.

Lutjeharms, J. R. E., and A. L. Gordon, Shedding of an Agulhas ring observed at sea, *Nature*, *325*, 138–140, 1987.

McConathy, D. R., and C. C. Kilgus, The Navy Geosat mission: A review, *Johns Hopkins APL Tech. Dig.*, *8*(2), 1987.

Menard, Y., Observation of eddy fields in the northwest Atlantic and northwest Pacific by Seasat altimeter data, *J. Geophys. Res.*, *88*(C3), 1853–1866, 1983.

Robinson, A. R. (Ed.), *Eddies in Marine Science*, 609 pp., Springer-Verlag, New York, 1983.

Sandwell, D. T., and B. H. Zhang, Global mesoscale variability from Geosat Exact Repeat Mission: Correlation with ocean depth, *J. Geophys. Res.*, *94*(C12), 17,971–17,984, 1989.

Stanley, H. R., The GEOS-3 project, *J. Geophys. Res.*, *84*(B8), 3779–3783, 1979.

Stewart, R. H., *Methods of Satellite Oceanography*, 360 pp., University of California Press, Berkeley, 1985.

Tapley, B. D., and G. H. Born, The Seasat precision orbit determination experiment, *J. Astron. Sci.*, *XXVII*(4), 315–326, 1980.

Tapley, B. D., G. H. Born, and M. E. Parke, The Seasat altimeter data and its accuracy assessment, *J. Geophys. Res.*, *87*(C5), 3179–3188, 1982.

Wunsch, C., and E. M. Gaposchkin, On using satellite altimetry to determine the general circulation of the oceans with application to geoid improvement, *Rev. Geophys.*, *18*(4), 725–745, 1980.

Wyrtki, K., L. Magaard, and J. Hager, Eddy energy in the oceans, *J. Geophys. Res.*, *81*(15), 2641–2646, 1976.

Zhang, B. H., Geosat/ERM altimeter data analysis for the determination of the global oceanic mesoscale variability, Ph.D. dissertation, Univ. of Tex. at Austin, Dec. 1988.

Zlotnicki, V., L. L. Fu, and W. Patzert, Seasonal variability in global sea level observed with Geosat altimetry, *J. Geophys. Res.*, *94*(C12), 17,959–17,969, 1989.

R. S. Nerem, Goddard Space Flight Center, Code 626, Greenbelt, MD 20771.

D. T. Sandwell, Scripps Institute of Oceanography, Geological Research Division A-020, La Jolla, CA 92093.

C. K. Shum, R. A. Werner, and B. D. Tapley, Center for Space Research, The University of Texas at Austin, Austin, TX 78712.

B. H. Zhang, P. O. Box 8701, Space Science and Applications Research Center, Chinese Academy of Sciences, Beijing 100080, People's Republic of China.

(Received August 18, 1989;
revised April 6, 1990;
accepted April 18 1990.)

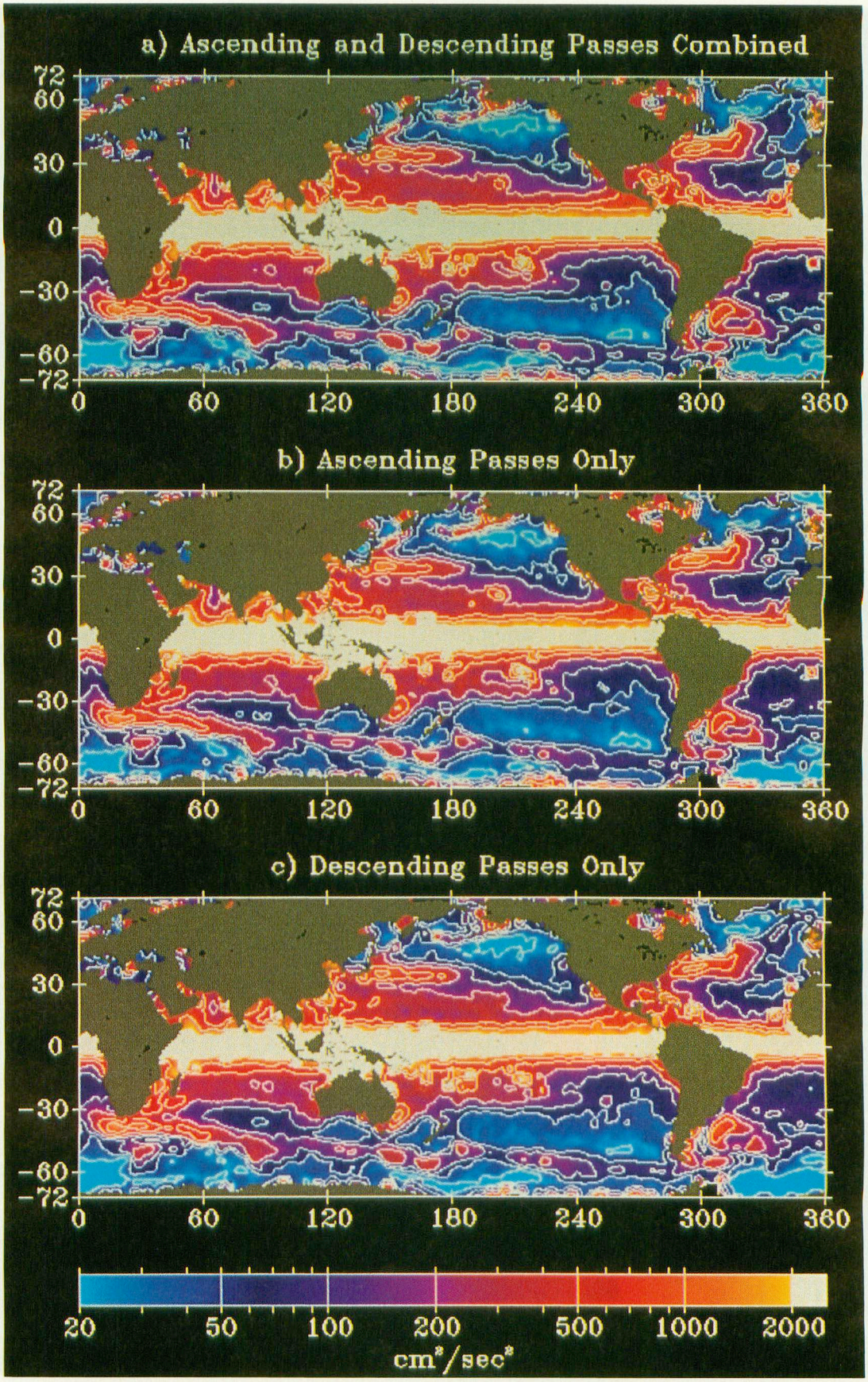

Plate 1 [*Shum et al.*]. Eddy kinetic energy maps generated using 2 years of Geosat altimeter data (November 1986 through November 1988) for (*a*) ascending and descending passes, (*b*) ascending passes only, and (*c*) descending passes only. Similarities between Plates 1*b* and 1*c* support the isotropic assumption that along-track and cross-track rms velocity variability are identical.

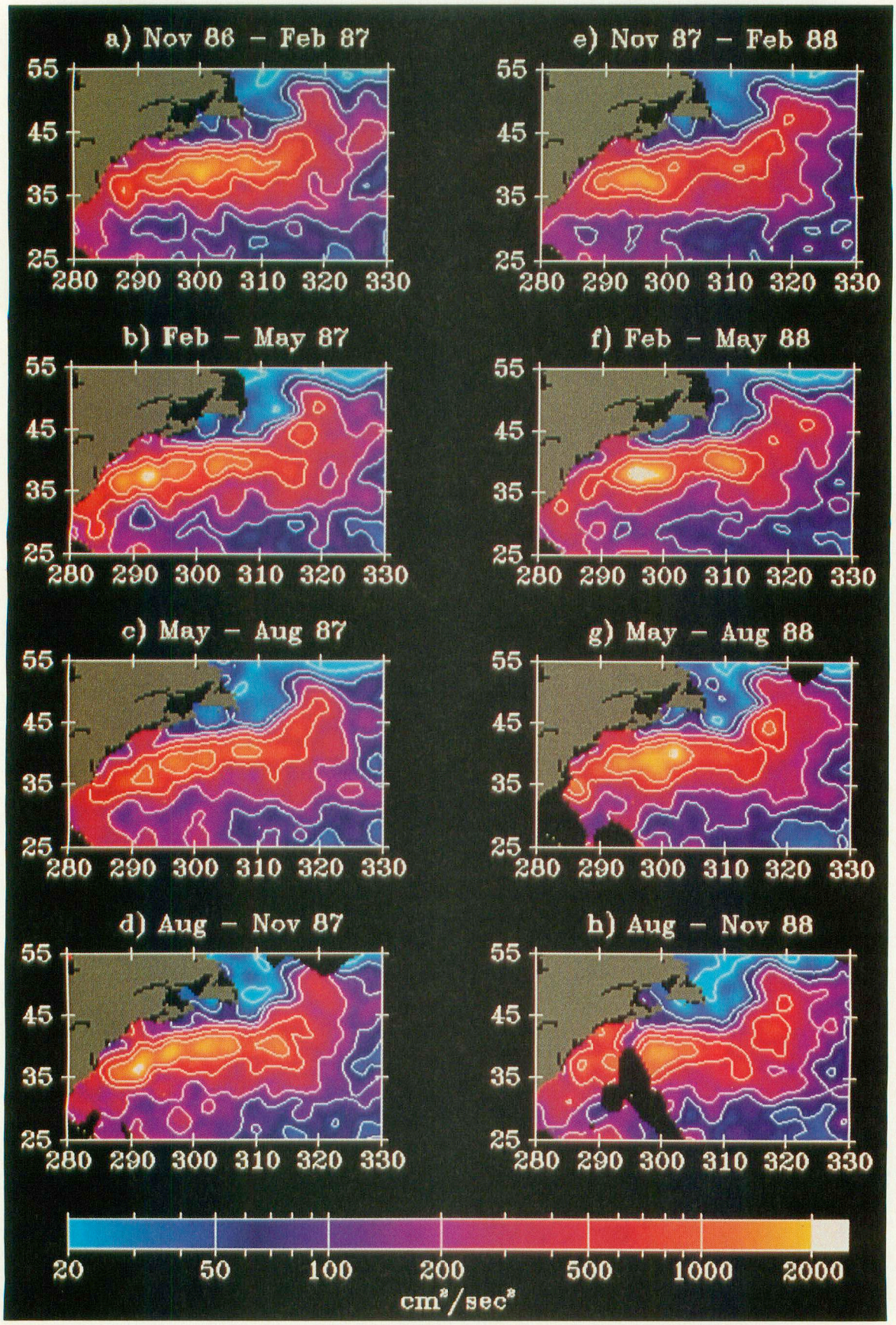

Plate 2 [*Shum et al.*]. (*a–h*) Eddy kinetic energy maps averaged over 3-month intervals for the Gulf Stream current system. The Gulf Stream seems delineated by 500-cm^2/s^2 eddy kinetic energy levels. Annual cycles of average position and shape are evident, but strength and location of maximum variability do not repeat.

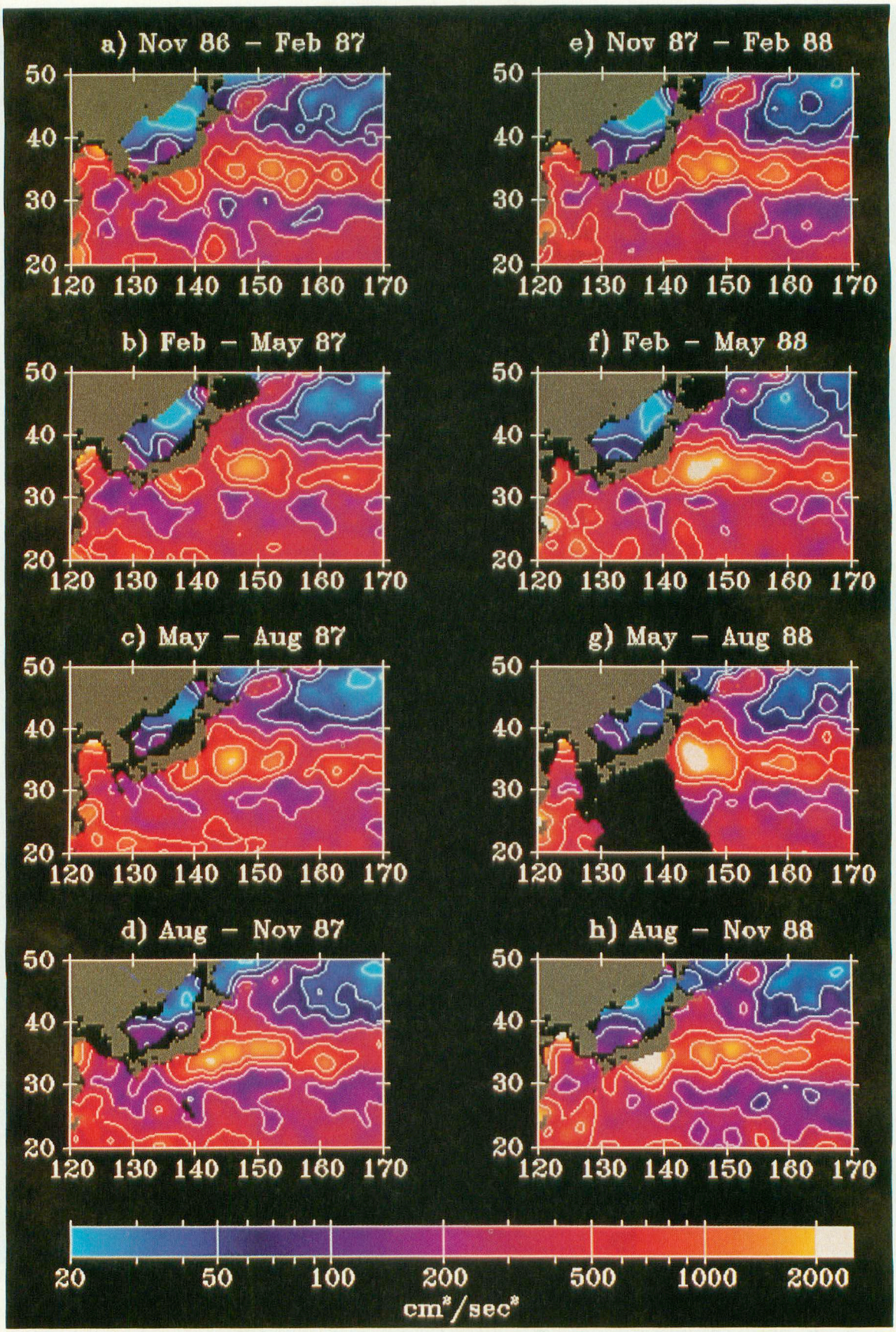

Plate 3 [*Shum et al.*]. (*a–h*) Eddy kinetic energy maps averaged over 3-month intervals for the Kuroshio current. High values of eddy kinetic energy (>1000 cm^2/s^2 correspond to the meandering of the current front, especially between the Kuroshio and Oyashio fronts (35°–40° N, 140°–155° E).

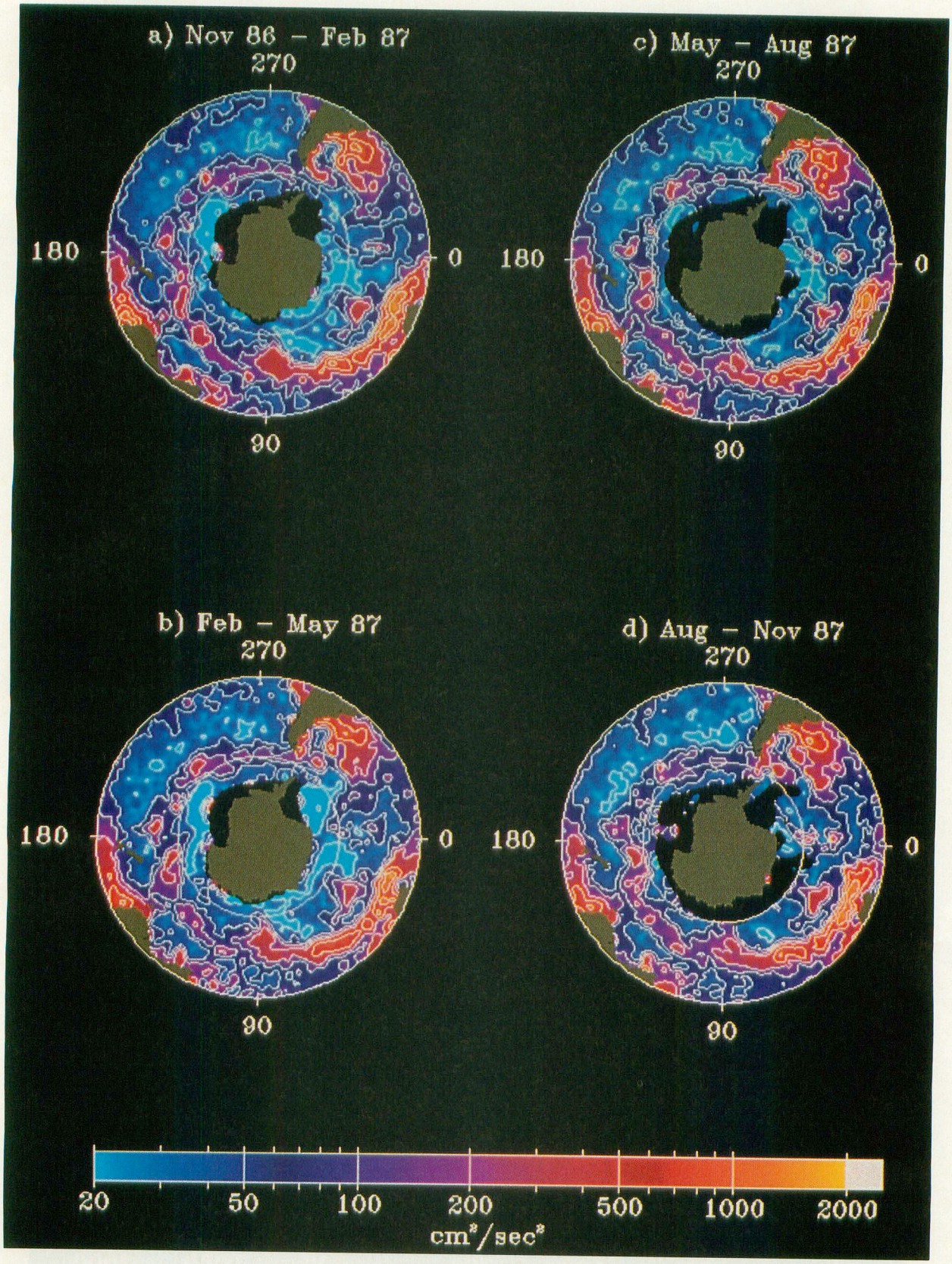

Plate 4 [*Shum et al.*]. (*a–h*) Eddy kinetic energy maps averaged over 3-month intervals for the Antarctic region. Eddy kinetic energy in the Antarctic Circumpolar Current generally reaches 500 cm^2/s^2, and energies exceeding 1000 cm^2/s^2 appear in the Agulhas, Brazilian, and East Australian currents. There seems to be little seasonal variation in the position and magnitude of the ACC's eddy kinetic energy.

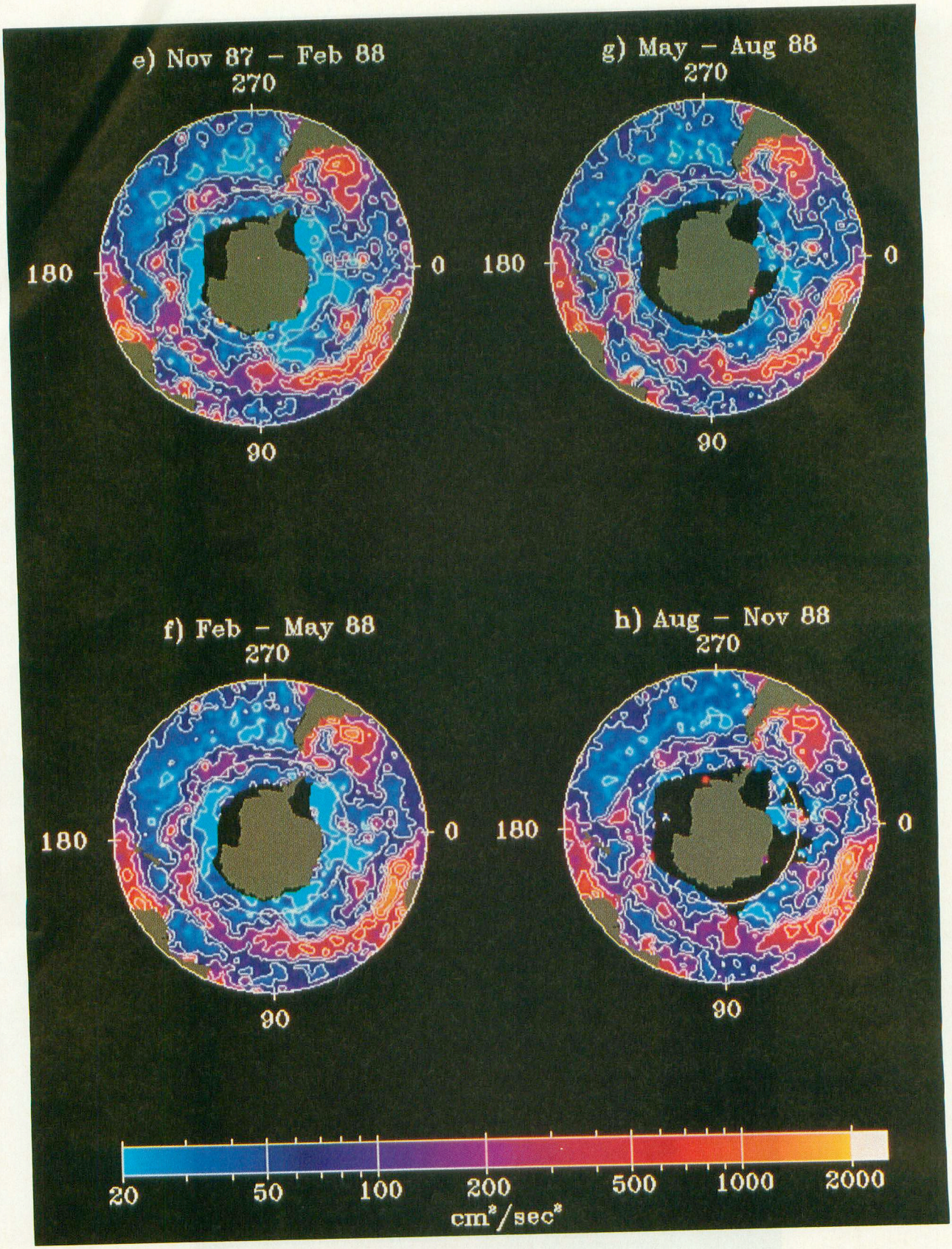

Plate 4 [*Shum et al.*]. (continued)

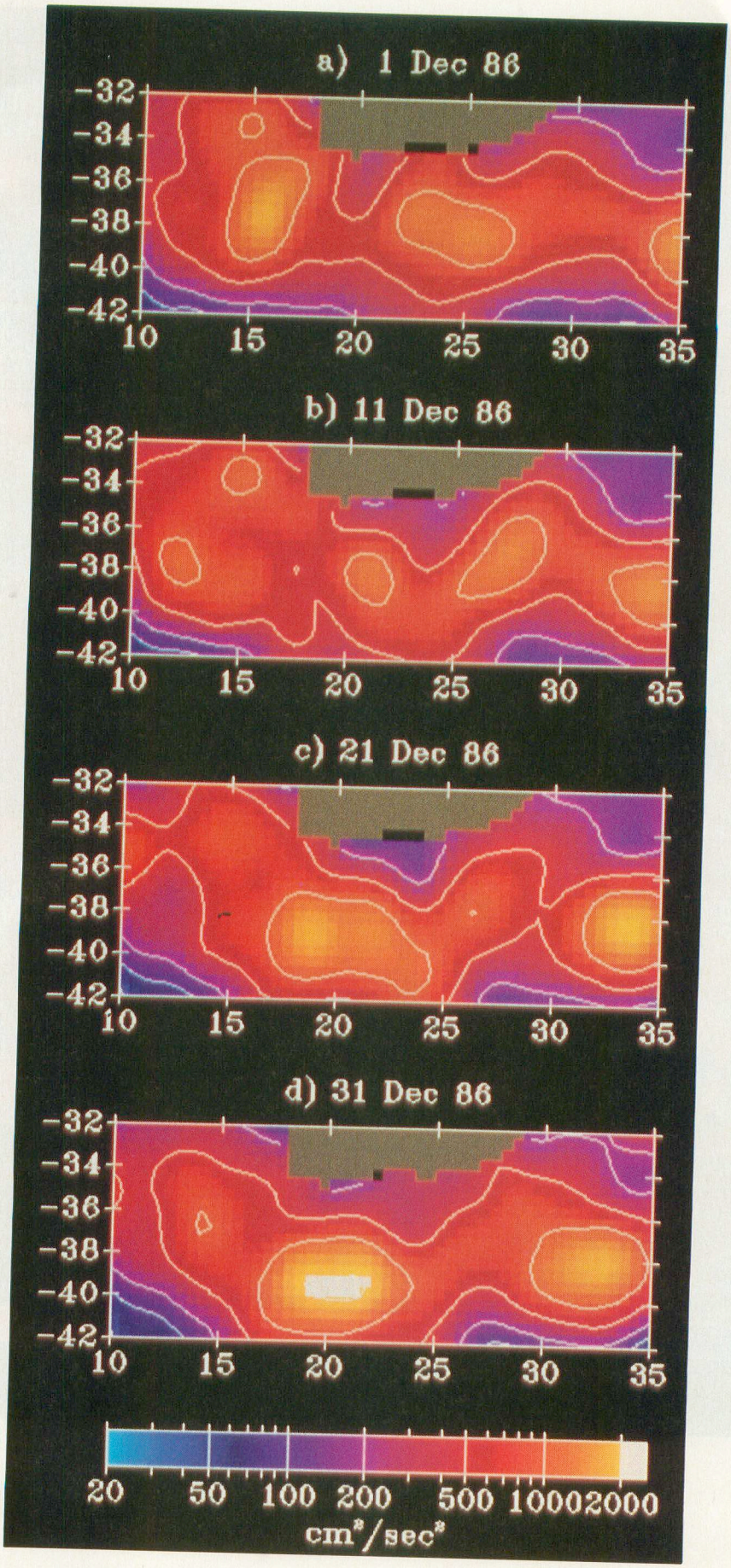

Plate 5 [*Shum et al.*]. (*a–d*) Eddy kinetic energy snapshots generated at 10-day intervals for the Agulhas retroreflection region. Eddy features evolve quickly in strength and position.